A comprehensive methodology to screen metal-organic frameworks towards sustainable photofixation of nitrogen

Amro M.O. Mohamed, Yusuf Bicer

Computers and Chemical Engineering 144 (2021) 107130

Contents lists available at ScienceDirect

Computers and Chemical Engineering

journal homepage: www.elsevier.com/locate/compchemeng

A comprehensive methodology to screen metal-organic frameworks towards sustainable photofixation of nitrogen

Amro M.O. Mohamed*, Yusuf Bicer

Division of Sustainable Development (DSD), College of Science and Engineering (CSE), Hamad Bin Khalifa University (HBKU), Qatar Foundation (QF), Education City, P.O. Box: 34110, Doha, Qatar

ARTICLE INFO

Article history:
Received 29 April 2020
Revised 13 September 2020
Accepted 18 October 2020
Available online 19 October 2020

Keywords:
Nitrogen fixation
Photocatalysis
Solar energy
Ammonia
Throughout-put screening
Computational tools

ABSTRACT

Distinct photoactive material compositions have been investigated starting from the mid-70s to reduce energy and pollution associated with ammonia synthesis. Hitherto, photocatalysts suffer from low ammonia yield and incomprehensive understanding of the mechanisms. The target of this research is to develop a systematic and comprehensive approach to screen and design durable and efficient metal-organic frameworks (MOFs) as catalysts to drive the photofixation of nitrogen at atmospheric conditions. This work discusses the available databases in the context of photocatalysis for the first time and reviews essential descriptors by incorporating Quantum Mechanics and molecular simulation techniques, taking into consideration sustainability aspects. As a result of a study on Hypothetical MOFs, $Zn_3(BTC)_2(C_6H_5)$ has shown to satisfy the requirement for photofixation of nitrogen, using hydrogen and nitrogen as inputs, to ammonia. Comparison between $Zn_3(BTC)_2(C_6H_5)$ and NH_2-MIL-125(Ti) has been made based on geometrical, bandgap, diffusion coefficients, adsorption properties and life cycle assessment analysis of the production phase.

1. Introduction

Ammonia is considered the primary precursor to fertilizers (Bencic, 2001). In addition, ammonia has emerged as a potential alternative of energy carrier and hydrogen vector. Several advantages make ammonia a viable medium to store solar energy; these are, ease of liquefaction, distribution network and infrastructure availability, handling experience, narrow flammability and ease of handling and storage. Currently, extensive use of energy (1.2% of the primary energy consumption) and extreme emissions of pollutants (0.93% of global greenhouse gas emissions) (Gilbert and Thornley, 2010) are associated with the production of the raw materials necessary for commercial ammonia production through the well-known Haber-Bosch process. Through the utilization of renewable energies, the production of ammonia can be achieved, avoiding energy-intensive and pollutant routes. Photocatalytic propelled fixation of nitrogen at a benign condition is the ultimate goal.

The natural nitrogen fixation process motivated researchers to invest time in developing systems that operate under ambient conditions to produce ammonia. In the bigger picture, three main classes of photocatalysts have been explored. These are bio/inorganic hybrid (Brown et al., 2016), biomimetic chalcogels (Banerjee et al., 2015) and pure inorganic semiconductors doped with metallic and nonmetallic dopants. Recently, carbon-based materials have been investigated for the fixation process employing nitrogen vacancies (Hu et al., 2016, Dong et al., 2015, Lashgari and Zeinalkhani, 2018). Different systems have been investigated to drive and promote the photofixation of nitrogen: metal oxides, metal sulfides, Bismuth oxyhalides, carbonaceous, and others (Chen et al., 2018).

A photocatalyst is a compound or a material which promotes the reaction of substrates into products by utilizing light energy (Turro et al., 2010). Usage of a material's light absorption capability in raising the rate of chemical reactions defines photocatalysis (Augugliaro et al., 2019), (Braslavsky Silvia et al., 2011). The vast majority of photocatalysts are either organic or metallic complexes (Navalón and García, 2018). Organic compounds suffer from the loss of activity due to degradability issue, but the synthesis is reliable and offers the possibility to modify their photophysical and photochemical properties by introducing substituents on the chromophore. On the other hand, inorganic structures provide the essential stability under irradiation and are very durable; however, it is difficult to tune and control the properties as in the organic compounds.

* Corresponding author.
E-mail address: ammohamed@hbku.edu.qa (A.M.O. Mohamed).

https://doi.org/10.1016/j.compchemeng.2020.107130

Metal-Organic Frameworks (MOFs) solve the issues concerning organic compounds and inorganic structures, avoiding degradability and granting tunability. MOF photocatalytic performance has been tested in several applications (Zhang et al., 2017). The review discusses MOFs for renewable energy and environmental applications and summarizes the list of applications in which MOFs are used. Applications include photocatalytic and electrocatalytic processes. These include hydrogen evolution reaction (HER), oxygen evolution reaction (OER) and oxygen reduction reaction (ORR), photocatalytic CO_2 reduction, batteries and supercapacitors. Recently, MOFs application was extended to fixation of nitrogen to produce ammonia (Huang, 2020; Li et al., 2020). The difficulty in modelling heterogeneous catalysis can be overcome or eased if the surface is determined definitely as in the case of MOFs. MOFs are highly crystalline materials that can be synthesized to an exacting specification, including the setup of identical active site at uniform distances.

Several contributions in the literature had successfully investigated MOFs for visible light activity with the use of sacrificial electron donor or acceptors (Horiuchi et al., 2012, Wang et al., 2012, Wei et al., 2012, Che et al., 2012). MOFs, due to their unique coordination and an immense library of components, are considered as a testbed to engineer molecular solids for light-harvesting applications (Thomas and Thomas, 2015). Some of the merit account of MOFs to facilitate catalytic properties are(Wang et al., 2012):

- MOFs allow facile separation of production, regeneration and re-use because of their open structure.
- Properties can be tuned and designed rationally through metal substitution, ligands replacement, and integration of functional groups.
- Single-site type of photocatalysts.
- The open structure nature facilitates the diffusion of reactants, and products are away from their precisely known active sites.

MOFs have been demonstrated to be photocatalytically active (Gomes Silva et al., 2010), (Silva et al., 2010). It is relevant to investigate the role of each part of the MOF towards photoactivity. Silva et al. mentioned that if the organic linker used in the construction of the MOF is active in the visible light region, one would expect that the MOF should have activity under visible light as a consequence, which indicates that the linker harvests the light, and the energy is transferred to the metal node (Silva et al., 2010). It was explained that the most relevant charge transfer in MOFs is due to the ligand to metal transfer rather than metal to organic linker transfer (Dhakshinamoorthy et al., 2016), (Alvaro et al., 2007). It has been shown that upon the addition of Zn^{2+}, transient signal attributed to the triplet excited state of terephthalate in water underwent static and dynamic quenching (Alvaro et al., 2007). MOFs should exhibit some intermediate between the high electron mobility of n-type semiconductors and slow electron mobility of an array of independent transition metal complexes (Navalón and García, 2018). It was claimed that the structure of MOF has a significant role in determining the nature of charge separation in MOFs, either as a semiconductor or assembly of independent complexes (Dhakshinamoorthy et al., 2016).

Photocatalytic efficiency is affected by the efficiency of electron transfer from the liner to the metal nodes (Dhakshinamoorthy et al., 2016). Theoretical studies attempted to relate the overlap between molecular orbitals to photocatalytic activity (Dhakshinamoorthy et al., 2016), (Nasalevich et al., 2016), (Butler et al., 2014). If an overlap between the electron density of the lowest unoccupied molecular orbital of the linker and the empty orbital of the metal nodes, then electron transfer from the metal to the ligand should be efficient. As most MOFs are highly porous materials which consequently allow for the diffusion of substrates, charge migration speed is not of high prominence, therefore, studying the semiconductors behaviour and link to MOFs for photocatalysis application is not vital (Navalón and García, 2018).

The importance of guiding and complementing the experimental work with simulation results was realized when researchers exploited zirconium on zirconium oxide film to replace Ru co-catalyst (Oshikiri et al., 2016). The choice of eliminating Ru as a co-catalyst is that this element is known for active absorption of hydrogen which hinders the production of ammonia, which is supported by Density Functional Theory (DFT) calculations. Through related methods, Zr surface has been revealed as a surface which has higher selectivity towards nitrogen. In fact, the formation rate of ammonia increased by a ratio of 6 compared to the Ru previous case. Several studies included a DFT section in the contribution to explain and support a claim. For instance, Dong et al. solidified the point that nitrogen vacancies are the spots of nitrogen chemisorption, DFT calculations were employed to estimate the interactions between nitrogen and surface (Dong et al., 2015). Theoretical studies that combine computational work with experimental measurements in nitrogen fixation are scarce. Density functional theory is considered as the ideal fit in screening for photocatalyst candidates (Cinar, 2017) and also for exploiting the methodology to expand the knowledge on the mechanism under which the reaction takes place and products yield.

Infrared spectrum (800-3000 nm) constitutes more than half of the solar energy. Building materials that can harvest this relatively high wavelength light section in photocatalytic is therefore appealing. Also, it is necessary to understand the role of impurities in hindering the photocatalytic activity of a material. The main objective of this work is to prepare a methodology that assists in selecting MOFs from a MOFs based database in reaching a selection for nitrogen photofixation. In this work, macro, meso and micro levels are combined to arrive at a reasonable conclusion on a structure/property and structure/activity relationships in a photocatalysis application perspective. Also, a demonstration of the screening is shown considering hypothetical MOFs. As concluded by Hasnip et al. that computational exploration of materials space offers advantages over an entirely experimental attack (Hasnip et al., 2014).

1.1. Significance of the present study

Up to the authors' knowledge, this is the first computational work that is directed towards the investigation of MOFs for sustainable nitrogen photofixation process. The work intends to emphasize on MOFs being ideal for bridging the gap between photocatalysis and computational tools. Also, a discussion of available databases is used to highlight the potential of current libraries for photocatalysis applications. This paper incorporates life cycle thinking of the material synthesis and compares the environmental impact of MOF constitutes.

Moreover, a demonstration is reported, which screened the hypothetical MOFs database for the fixation process, considering a consecutive procedure. Given the preliminary requirement and calculations of required electronic properties, MOFs built from Zn_2 metal nodes, and trimetric acid ligands (BTC) functionalized with phenyl group are expected to be effective nitrogen fixation MOFs. The outcome, for the first time, highlights this material for sustainable energy application, more specifically, ammonia production. Geometrical, diffusion and adsorption properties are computed using multiple molecular simulation techniques. The parent Zn-BTC has also been compared to MIL-125(Ti) concerning environmental impact using LCA based on synthesis routes. Throughout the screening process, the role of several functional groups on the electronic properties of MOFs was identified, which can guide the future synthesis of MOFs towards sustainability-related photocatalytic applications such as water splitting and CO_2 reduction. In

the following section, the list of possible and related criteria will be discussed in the context of light absorption and photocatalysis.

2. Methodology and parameters building process

Several groups contributed significantly to the state-of-the-art methodology screening of MOFs and to make the process more efficient for the past decade. Jiang reviewed the recent publications on screening different MOFs databases and subsets towards CO_2 capture (Jiang, 2019). The short review highlighted the successful implementation of the screening process of MOFs into experimental testing of performance accomplished by Chung et al. (Chung et al., 2016). One of the most relevant screening paper was written by Azar et al. (Azar et al., 2019). The work examined Cambridge Structural Database (CSD) MOFs towards H_2/N_2 binary separation with 30:70 ratio (Azar et al., 2019) using methods to quantify permeability in membranes. It was reported that all MOFs have adsorption selectivity towards N_2, which make it nearly ineffective towards diffusion selectivity. H_2/N_2 selectivities of MOF membranes were slightly lower in the mixture case compared to the ones obtained at the infinite dilution. The H_2/N_2 ideal adsorption based selectivity of MOFs various between 0.3 and 0.7.

The screening process methodology relies on the database used to identify the desired materials. There are three central databases used for this process. The first database was designed by Wilmer et al., where 102 building units are used to design 137953 hypothetical MOFs (HMOFs) (Wilmer, 2012). The database contains mixed ligand MOFs while mixed metal is unavailable. Also, novel materials with different nodes have to be tested for stability before the performance check. The second one is the computation-ready experimental (CoRe) MOFs (Chung et al., 2014). This database offers materials that have been synthesized, and the structures are derived from experimental crystallographic data. The third database is the Cambridge Structural Database (CSD), which also provides experimental deposited structures from researchers/scientists.

The catalytic or photocatalytic applications involve numerous parameters than those involved in screening for separation processes. Especially photocatalytic activity and efficiency include several stages of material light absorption, charge excitation and separation. In this section, several descriptors will be discussed, and consequently, parameters will be highlighted and withdrawn, which can be used for the process of screening MOFs for photocatalytic activity towards nitrogen fixation. Fig. 1 provides a holistic approach into the different layers required to be assessed before selecting a MOF to perform nitrogen photofixation. In addition to electronic related characteristics, the following steps must be taken into account when investigating a photocatalytic reaction (Augugliaro et al., 2019):

1 Diffusion of reactants to the photocatalysts through the boundary layer
2 Diffusion of reactants into the pore surface
3 Photoadsorption of reactants on the pore surface
4 Photoreaction
5 Photodesorption of reactants on the pore surface
6 Diffusion of products out of the pore surface
7 Diffusion of products away from the photocatalysts through the boundary layer

Nowadays, due to the enormous increase in computational power in hand, computational science can contribute significantly to the development of catalytic systems. Computational works provide a significant contribution to the field of catalysis, mainly because transition states can be observed using DFT, which would have been unattainable in experimental setups. Also, the dynamics of the system and opportunities for improvement are feasible with methods such as Molecular Dynamics (MD) and Monte Carlo (MC). Other assessment methods combine reaction pathways, catalytic cycles and process kinetics modelling.

2.1. Adsorption and diffusion

MC and MD simulation types of force field based approaches calculate a broad range of properties, thermophysical, transport, and structural, while quantum mechanical calculations are more appropriate to examine chemical properties such as bond breakage and formation (Leach, 2001), (Dubbeldam et al., 2016). MOFs are mostly assumed to be rigid during the process of evaluation adsorption and diffusion of small molecules (typically studies in the literature). Models used for MOFs is used through parameters found in generic force fields to save computational time. Atomic charges can be estimated through DFT and semi-empirical methods. Therefore, screening can be done neglecting the atomic charge estimation for rapid calculations. On the other hands, substrates are modelled through more specific force fields; for instance, N_2 and NH_3 are mostly modelled using TraPPE force field (Martin and Siepmann, 1998), (Zhang and Siepmann, 2010).

An equation is built to recognize steps 3 to 5 of the heterogeneous catalysis steps. Adsorption parameter (Eq. 1) reflects the production of ammonia in the system; which is evaluated by subtracting the excess adsorption value from the stoichiometric value. One could include other adsoprtion based descriptors such as the adsorption selectivity. Nitrogen is reacted according to the chemical reaction stoichiometry. Thus the product is evaluated from a thermodynamic point of view, as this does not consider kinetics or light adsorption efficiency or dissociations of reactants.

$$\begin{aligned} AdsorptionParameter &= StoichemtricValue \\ &\quad - ExcessAdsorptionValue \\ &= 2 \times N_{N_2}^{Excess} - N_{NH_3}^{Excess} \end{aligned} \tag{1}$$

Adsorption can be investigated by Grand Canonical MC (GCMC) calculations. GC ensemble simulates an open system where both the number of particles and the internal energy are the fluctuating properties. Henry's constants (K^0) can be evaluated using the Widom particle insertion method (Frenkel and Smit, 2002).

Locating adsorption sites and determining the heat of adsorption (Q_{st}) are two quantities that have to incorporate when studying adsorption in nanoporous materials which can be obtained readily from the computations. Location of adsorption can be observed and assessed via the introduction of radial distribution function (RDF). RDF is prepared by calculating the distance between particle pairs. The use of this function can be used by plotting the distance between nitrogen atom in molecular nitrogen and the active site of the structure at operating pressure and most importantly at infinite dilution limit. Binding energy can be determined from DFT simulations and can also be found through the computation of enthalpy of adsorption at infinite dilution (ΔH) as follows:

$$\Delta H = \Delta U - RT = \langle U_{hg} \rangle - \langle U_h \rangle - \langle U_g \rangle - RT \tag{2}$$

where ΔU is the change in internal energy calculated by subtracting the host and adsorbate energies from the host-gas interaction.

The most favourable adsorption site is the one corresponding to the highest exothermic energy. In the case of hydrogen and nitrogen, mole compositions of the gas phase can be reflected in the simulations from the stoichiometry of the reaction. However, to maintain mole composition of the stoichiometry identical to the gas phase, additional hydrogen might be required as structures will have selection adsorption of adsorbates over another, especially in the case of ammonia production as demonstrated by reactive MC simulations (Turner et al., 2001).

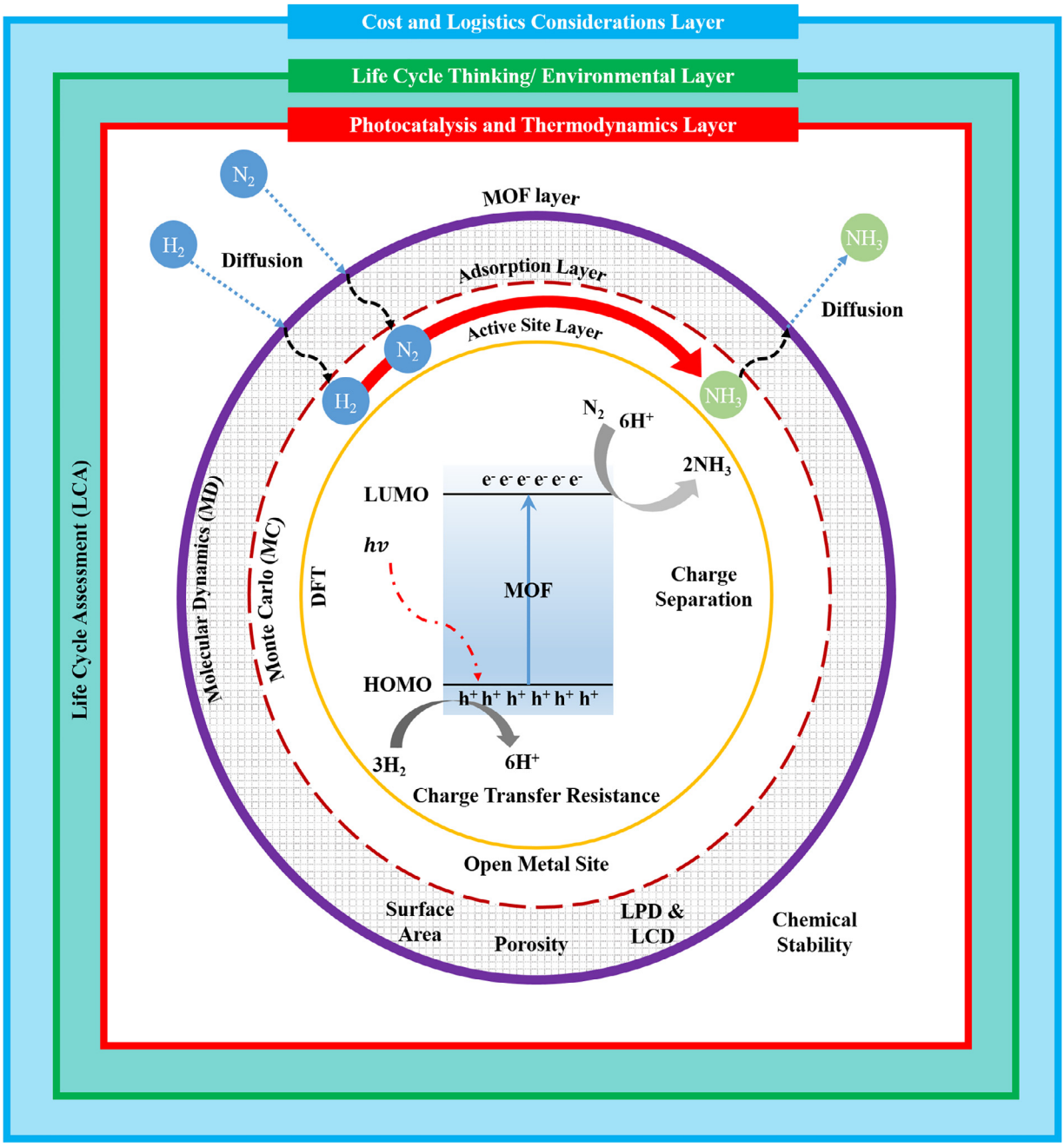

Fig. 1. Various layers to characterize MOFs for sustainable nitrogen photofixation.

Determination of molecular diffusion can be accomplished using molecular dynamics (MD). Mean square displacement (MSD) of a particular molecule is obtained at the end of an MD simulation. The slope of MSD data are used in the following equation:

$$MSD(t) = \frac{1}{N}\left\langle \left(\sum_{j=1}^{N} \left[r_j(t) - r_j(0) \right] \right) \right\rangle^2 \quad (3)$$

where, N is the number of molecules, $r_j(t)$is the position vector of the molecule of species j at time t. Self-diffusivity is found from MSD(t) by the Einstein relation as follows:

$$D_{self,i} = \lim_{t \to \infty} \left(\frac{MSD(t)}{2dt} \right) \quad (4)$$

As a result of the selection of materials which possess PLD larger than the kinetic diameter of ammonia (the product), one can assume all of the product from adsorption analysis is observed. The adsorption of nitrogen might be affected by adsorption of hydrogen; therefore, reactants adsorption computations are suggested to be performed under binary mixtures conditions. Calculations of molecular diffusivity are aimed to ensure that self-diffusivities are greater-than 10^{-8} cm^2/s and to compare between candidate materials.

2.2. Photo-sensitivity of photocatalysis

Step 5 requires photoabsorption and charge excitation. Recently developed DFT codes can compute a decent number of essential properties; structural, chemical, optical, spectroscopic, elastic, vibrational and thermodynamic phenomena (Hasnip et al., 2014). DFT underlying principle is that the total energy of the system

Table 1
Potential (V) vs SHE for the three steps 2e− reduction of nitrogen at atmospheric conditions.

Reaction	Potential (V) vs SHE
$\mathbf{N \equiv N + 2H^+ + 2e^- \rightarrow H - N = N - H}$ (**Diimine**)	-1.260
$\mathbf{H - N = N - H + 2H^+ + 2e^- \rightarrow H_2N - NH_2}$ (**Hydrazine**)	+0.434
$\mathbf{H_2N - NH_2 + 2H^+ + 2e^- \rightarrow 2\ NH_3}$ (**Ammonia**)	+0.995
$\mathbf{H_2 \rightarrow 2H^+ + 2e^-}$	0.000

is a unique functional of the electron density (Hohenberg and Kohn, 1964). DFT is used as an exploratory tool towards materials discovery and computational experiments (Hasnip et al., 2014). It is essential to be able to predict oxidation and reduction potentials of molecules and structure as it has an immediate impact in studying those molecules in several applications, including photocatalysis. More specifically, determining the highest occupied molecular orbital (HOMO) and the lowest unoccupied molecular orbital (LUMO) energies can provide the required information to design novel and efficient materials for solar energy harvesting.

The importance of the HOMO and LUMO levels lies on it being the place where charge generation, separation and transfer processes take place. Electron transfer from the donor to the acceptor requires donor's LUMO level to be above that of the acceptor. The hole transfer from the acceptor to donor requires that the donor's HOMO level be above that of the acceptor (Leonat et al., 2013). HOMO represents the energy required to extract an electron from a molecule, LUMO represents the energy needed to inject an electron to a molecule (Leonat et al., 2013). Another critical parameter is the Fermi level, which provides knowledge about the probability distribution of electron occurrence between HOMO and LUMO. Considering a three steps $2e^-$ reduction process, the potentials of reactions involved in the nitrogen fixation are presented at 25°C vs standard hydrogen electrode (SHE) in Table 1.

The captured light quantifies the portion of sunlight that a structure can absorb. Absorption of light is a quantity, which can be calculated using the bandgap value. It is the integration of the solar spectrum between near zero wavelength to the bandgap corresponding wavelength. Estimation of this quantity is derived by plotting wavelength (nm) versus the integration of the solar spectrum. The design criteria of the bandgap should be between 1.5 and 2.75 eV. The lower limit is estimated as the nitrogen fixation threshold of 1.26 eV plus 0.25 eV. The lower limit realistically may have to be even higher, but for the sake of screening, this should be enough. The higher limit is fixed at 2.75 eV to ensure high light capture percentage and efficiency. Concerning the band position, the following pair of inequalities must be satisfied for a material to be considered.

$$VB_{edge} > 0.00\ V\ vs\ SHE\ and\ CB_{edge} < -1.26V\ vs\ SHE$$

2.3. Catalytic and structural stability

Rosen et al. introduced DFT obtained properties in identifying MOFs as a catalyst. The work published in 2019 demonstrated that the favorability of formation of metal-oxo is indicative for methane activation capability of 60 open metal site MOFs using radical rebound mechanism (Rosen et al., 2019). They showed that the active site heat of formation is the parameter required to obtain information regarding reactivity and site stability. For the nitrogen fixation process; the following reaction scheme can be considered (Rosen et al., 2019);

$$\Delta E_N = E_{MOF-N} - E_{MOF} - \frac{1}{2}E_{N_2} \quad (5)$$

$$\Delta E_H = E_{MOF-NH_3} - E_{MOF-N} - \frac{3}{2}E_{H_2} \quad (6)$$

where ΔE_N and ΔE_H demonstrate active site formation energy and H-affinity using N_2 and H_2 as references, respectively.

Several selection points have to be considered during the screening or in the analysis of results as summarized below:

1 Specific surface area and open metal sites: the higher the surface area, the better the dispersion. If the substrate and product are small, then an area of $1nm^2$ per active site is sufficed. An assumption can be made that metal node is the active site in the MOF.
2 Substrate accessibility can be measured using molecular probes of different sizes; through this, we can determine the fraction of surface area that this substrate can access. Zeolites and MOFs alike, have a channel and cage structure. In such cages, some of the substrate or product may be trapped inside the pores.
3 The heat of formation can be used as an indicator of the material's thermal and chemical stability (Emery and Wolverton, 2017), (Petrovic et al., 1993). High energy compounds are considered less stable. Also, mechanical properties such as shear modulus and Young's modulus are used to evaluate the mechanical resistance of a material (Mouchaham et al., 2018).

2.4. Environmental, geopolitical and economic aspects

One of the main pillars of sustainable energy is the environmental perspective. Life cycle assessment of materials is an essential part of selecting those for better management towards sustainable applications. The study should reflect upon a qualitative or quantitative measurement of environmental load. For rapid screening, a qualitative measure can be used; for instance, a comparison of the metal nodes. From the quantitative point of view, precursors used to prepare both organic linker and metal node have to be studied in an LCA environment. In other words, a given material is compared to another merely by quantifying the extraction and yield percentage. A single available research paper on LCA of MOFs was published in 2017 (Grande et al., 2017). It presented a cradle-to-gate LCA study conducted to evaluate four distinct routes to produce MOF-74. The work concluded that avoiding solvents in the preparation stage is necessary to minimize environmental impact. The study assumes that all the MOFs in the study are prepared in the same manner. Thus, extraction and yield percentage are controlling the results. Initial LCA results can be used for preliminary selection; specific LCA has to be done in later stages.

Input from LCA into the screening process has to be through the identification of the least environmentally detrimental metal. Selection can be accomplished through normalization of main impact categories in global warming potential (GWP) and others alongside (Armor, 2011) abundance value and criticality assessment contribution [(Graedel et al., 2012, European Commission (EC) 2014, N. R. C. 2008)]. Several studies have been conducted to investigate the potential of using various metals in sustainable catalysis from two aspects, supply risk (SR) and vulnerability to supply restriction (VSR) at the global and national (US) levels (Nuss et al., 2014, Nassar et al., 2012, Harper et al., 2015). An example is discussed here to select among the first line of transition metals of the periodic table. Considering five main impact categories; (1) GWP, (2) cumulative energy demand, (3) terrestrial acidification, (4) freshwater eutrophication, and (5) human toxicity, a comparison is made between the elements using data gathered from Nuss and Eckelman (Nuss and Eckelman, 2014).

An equation is used in order to combine all the five categories into one factor which calculates values relative to the maximum value in each category. A summation is run by considering the number of impact categories (n). The impact of each category is normalized to 1 relative to the maximum amount (impact) among the studied list of metals. It is important to note that this equation

demonstrates equal distribution and importance of all selected impact categories. Other work might select a material based on one or several categories, changing the weight or considering a different set of impact categories.

$$LCAfactor_i = \frac{\sum_1^n \left(\frac{Amount_i}{MaximumAmount}\right)}{n} \times 100\% \quad (7)$$

In this case, Scandium (Sc) is by far the worst metal among the list in all the categories, so essentially the rest of metals are compared relative to it. The lowest five in the list are; Mn (0.025%), Fe (0.027%), Ti (0.136%), Co (0.204%) and V (0.296%). The results show that Cr, Zn and Ni are 22, 43 and 54 times worse than Mn. Because Fe is more abundant than Mn and have close LCA factor; Fe is the best among the studied list of elements. One important note is that the production of Fe is higher than most of the metals and has to be included in the work through the criticality assessment. SR and VSR should be sufficient to modify the LCA factor. Also, it has to be pointed out that the LCA factor presented here does not include information regarding the organic linker. Some organic linkers are made from polycyclic aromatic hydrocarbons which are considered toxic. Therefore, an overall cradle-to-gate LCA comparison has to be used to compare the top materials, which includes organic linker and metal node.

The cost is a difficult factor to be estimated because the screening of MOFs may involve materials which have not been synthesized before. Also, MOFs are undergoing constant improvement in the synthesis process, which leads to a reduction in synthesis and preparation cost. Cost of MOFs has to be related strictly to both organic section and inorganic node. Cost of MOFs can be evaluated as the summation of costs of organic linkers and metal salts from the market assuming 100% yield from the reactants (Eqn 8); providing a piece of indirect information to compare MOFs from a cost perspective.

$$Costfactor = Costofbuildingblocks = \sum_{i=1}^{3} (costofmolecule)_i \quad (8)$$

where index *i* runs from 1 to 3 reflecting metal salt as the source of the metal, primary and secondary organic linkers used in the MOF's synthesis.

3. Results and discussion

The process of building a MOF based screening process can be envisioned through multiple consecutive or parallel steps. Determination of the sequence and type of screening depends on the volume of the structures in the database considered, intended application and accuracy pursued. Controlling factors also include available computational power and knowledge about the particular application and materials listed in the database. Considering consecutive based process reduces the burden of high computationally consuming steps. For instance, starting the process with identification of materials with desired structural adsorption properties, followed by quantum chemistry based calculations, most certainly reduce the computational time compared to evaluating the whole set using computationally demanded quantum chemistry calculations. Nevertheless, eliminating structures following structural or another step might lead to the exclusion of structures with sought-after electronic or mechanical properties.

On the other hand, comprehensive parallel screening has a primary advantage in helping the overall understanding of some structure/property relationships since the structures are not screened before the property determination step. Consequently, the computational cost is expected to be much higher because of testing the entire library regardless of essential properties. An integration between parallel and consecutive arrangements of steps might be considered the most preferable option. Proactive screening rather than a formerly set of constraints permits effective use of computational resources and establishing other uses for the materials in the database.

3.1. Available databases discussion

HMOFs databases are built from building blocks; thus, they offer the opportunity to find new materials for a particular application. The library has been exploited in screening MOFs for adsorption based and membrane-based separations (Wilmer et al., 2012), (Qiao et al., 2016). However, due to the nature and selection of the building blocks, it samples a limited portion of the structures. For instance, the HMOFs derived from 102 building blocks from the work of Wilmer et al. (2012) and only considered a single metal node and five forms of the metal node (Zn_4O, Zn_2, Cu_2, V_3O_3, and Zr_6O_6). Nowadays, mixed metal emerged as a new modification technique to tune MOFs properties. Mixed metal MOFs gained some interested because it provides another layer of tuning the properties of MOFs towards several applications including separation processes.

Besides, the number of dysfunctionalized organic linkers contained in the HMOFs library is limited. For instance, organic linkers used in the synthesis of Zeolitic Imadozilate Frameworks (ZIFs) are not covered in this library. Moreover, nodes built from Fe, Mn, and Co elements are not found in this library. LCA studies concluded the benign nature of Mn, and Fe extraction relative to other first-row transition metals. On the other hand, databases derived from experimental studies allow linking an already synthesized and characterized material to the desired function. One could say that this identification helps in material discovery as it highlights desired topologies based on metal nodes and linkers. Unlike HMOFs, these databases are growing continuously and include Mn, Fe, and Co based MOFs and mixed metal structures (Chung et al., 2019).

3.2. Screening of hypothetical MOFs database

An example is shown here to reveal the potential of such a screening process in identifying materials for nitrogen fixation or any other photocatalytic process. The process demonstrates the usage of hypothetical MOFs (HMOFs) as listed in the work of Wilmer (2012). In this work, the reduced form of the database is used (Chung et al., 2016). HMOFs have been screened in the literature for CO_2 capture (Wilmer et al., 2012), natural gas sweetening (Qiao et al., 2016) and H_2 capture (Gomez et al., 2014) applications. This screening is meant to reduce a relatively large database to a few hundred of potential structures. Towards sustainable photocatalysis applications, optical, structural, environmental, cost considerations have to be taken into account to select appropriate MOFs.

This case study intends to analyze the content of the database in a fast manner towards ammonia production from nitrogen and hydrogen. The library contains 51,163 MOFs out of which 47,211 are built with functional groups. The strategy followed in this work is illustrated in Fig. 2. First, the database is screened for open metal sites structures determined via zeo++ software (Willems et al., 2012). Zeo++ uses radii provided by the Cambridge Crystallography Data Center (CCDC). Out of the MOFs in the library, 324 MOFs possess open metal sites (0.63%). These MOFs were built exclusively from six different organic linkers and three metal nodes (Zn_2, Cu_2 and V_3O_3). Consequently, the resulting structures were divided into parent and non-parent structures. A parent structure indicates the absence of functionalization and interpenetration (Chung et al., 2016).

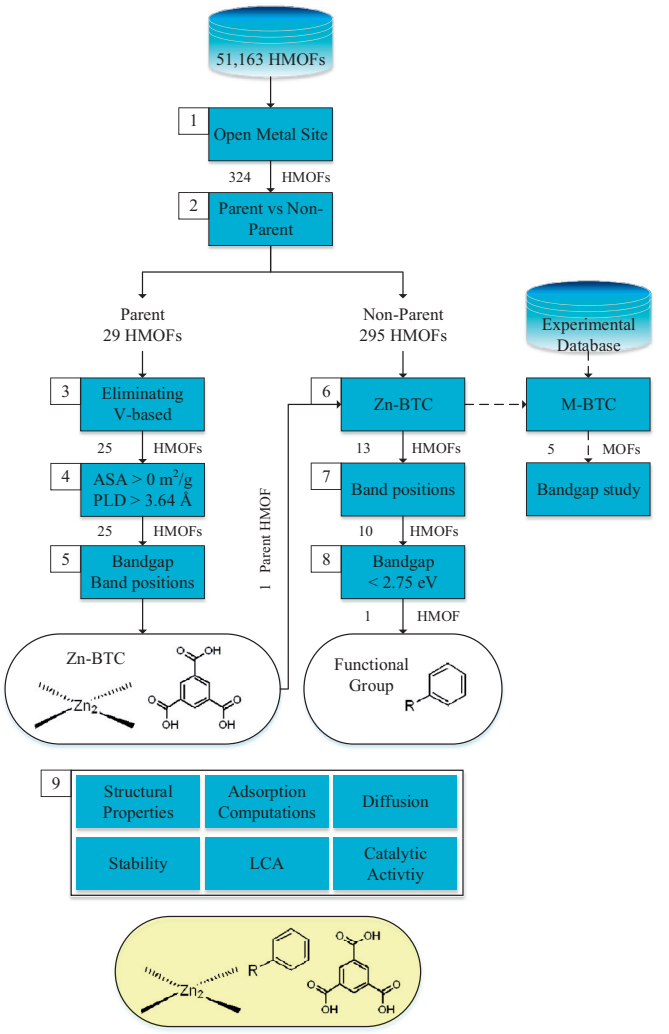

Fig. 2. Strategy and results summary of HMOF library screening process for photofixation of nitrogen.

The next two steps involve structural and environmental considerations. MOFs based on Vanadium were eliminated based on previous LCA discussion. Structures have to have accessible surface area higher than zero and PLD higher than the largest kinetic diameter among reactants and products (3.64Å). The result is 25 parent HMOFs which have an average 0.85±0.06 helium void fraction and have an average surface area of 4600±1432 m^2/g. Half of the structures were identified as Zn_2-based MOFs, where the other half is Cu_2-based MOFs. The cost of determining the geometrical descriptors of MOFs is not high; therefore, this step is ideal for initial of screening.

Electronic properties of interest in this work, bandgap and band edges were determined first for the 25 MOFs using electronic structure calculation carried on CP2K/QUICKSTEP package (The CP2K developers group 2008), (Hutter et al., 2014). CP2K has been used in screening processes of MOFs for building a database for Covalent-Organic Frameworks (COFs) (Ongari et al., 2019) and MOFs design for CO_2 hydrogenation (Ye and Johnson, 2015). In this work, the optimized Gaussian basis sets (MOLOPT) is being used (VandeVondele and Hutter, 2007). DZVP-MOLOPT-SR contracted Gaussian basis sets, and an auxiliary plane-wave basis set. The basis set is expected to perform in a wide range of chemical environments. The plane wave's cutoff is set to 300 Ry cutoff, and these are mapped on a 4-level multi-grid, with a relative cutoff of 60 Ry. Perdew Burke Ernzerhof (PBE) functional (Perdew et al., 1997), a generalized gradient appropriation (GGAs) method, was employed to represent exchange-correlation density functional. To represent core electrons, Geodecker Teter Hutter (GTH) PBE optimized pseudopotentials were used (Goedecker et al., 1996), (Hartwigsen et al., 1998).

Band edges were adjusted to SHE using $U^{\circ}_{(H^+/H_2)}$ (periodic boundary conditions) = 0.81 V (Liu et al., 2015). None of the 25 MOFs were identified to fit the nitrogen fixation reaction in terms of bandgap and band positions, and one structure has met the criterion of the bandgap. It is important to note that functionalization offers the capability of shifting the bandgap (Pham et al., 2014). From that standpoint, one of the 25 structures were selected being the sole structure with potentially adjustable band edges to fulfil the requirement of nitrogen fixation. It is a MOF built from benzene-1,3,5-tricarboxylic acid (H_3BTC) and Zn_2 metal nodes (bandgap ~ 3.6 eV) shown in Fig. 3.

The non-parent pot includes 13 distinct structures with the same building blocks with various functional groups Fig. 4. As a result of the variability in functional groups employed, the ranges of helium void fraction and surface area are 0.69±0.06 and 1940±265 m^2/g, respectively. The average accessible surface area has been reduced to 18% relative to the parent MOF. These structures were first analyzed with PBE functional and HSE06 hybrid functional for comparison in terms of accuracy and computational time. In addition to gradient-based methods, we incorporate the

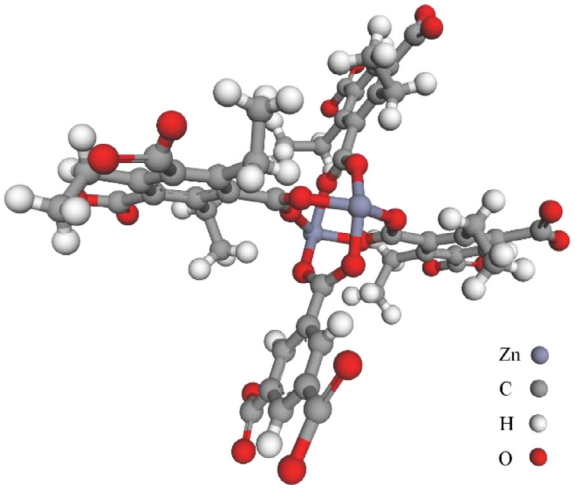

Fig. 3. Building unit of Zn-BTC.

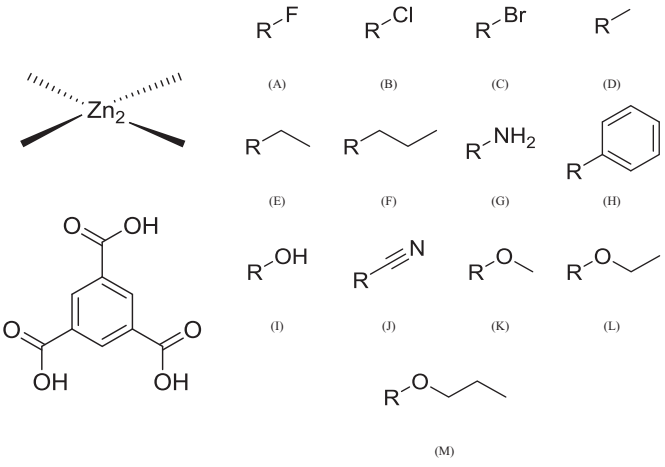

Fig. 4. Zn_2 metal node, BTC organic linker and functional groups used (A-M).

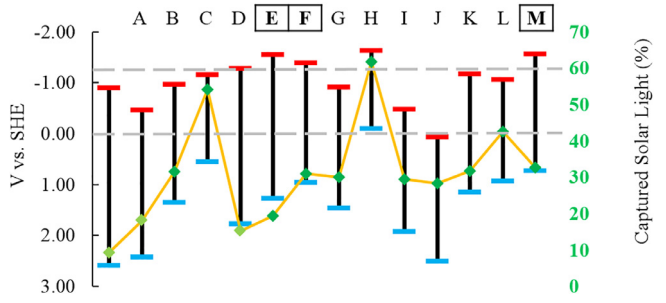

Fig. 5. Band energy plot of Zn-BTC and effect of functionalization using PBE functional versus the standard hydrogen electrode (SHE) potential.

use of hybrid functions as they have shown to solve the underestimation of bandgaps of GGAs through the cancellation of localization and delocalization errors (Mori-Sánchez et al., 2006). Here we use the efficient orbital transformation (OT) in implementation of HSE06 hybrid function were the screening parameter ($\omega = 0.11$) (Krukau et al., 2006) and Hartree-Fock (HF) mixing parameter equal to 0.25 (Perdew et al., 1996). HSE06 was used to show exceptional accuracy when it comes to bandgap prediction (Hendon et al., 2013). The auxiliary density matrix methods (ADMM) are employed in the calculation of HF exchange (Guidon et al., 2010). The MOLOPT basis set is also used in these computations, three Gaussian exponents for each valence orbital is used in the modelling of N, O, C and halogens atoms. Uncontracted basis sets are used for metal atom. The target accuracy for all SCF convergences is 1.0E-6.

From Fig. 5, one can observe the underestimation of bandgaps when considering gradient-based functionals. If one considers PBE functional, the majority of the structures satisfied the set criteria of the bandgap (11 out of 13, 84.6%). In this analysis, we use the results from HSE06 as it better estimates the bandgap of the parent structure $Zn_3(BTC)_2$, or simply Zn-BTC, (BTC^{-3} = 1,3,5-benzenetricarboxylate). However, only one of these functionalizations contributed to appropriate reduction to bandgap below 2.75 eV while modifying the conduction and valence band towards desired limits for the nitrogen fixation process. The structure is $Zn_3(BTC)_2$ associated with phenyl group (RC_6H_5), and the bandgap and position of HUMO and LUMO of the 13 structures are shown in Figs. 5 and 6 using PBE and HSE06, respectively. From the computational cost point of view, we have observed that HSE06 cost more than 100 times the time required to converge in PBE functional computations. Incorporation of HF exchange is responsible for the increase in the cost. The cost is also affected by the number of electrons in the system.

Fig. 6 shows how the weakest donating groups in methyl and ethyl groups slightly reduce the band; however, they shift the conduction band to higher negative values. Zn-BTC(Br) can be observed as a potential MOF for photofixation of nitrogen when water is the source of hydrogen as it has a bandgap of 3.00 eV and valence band that can oxidize water into hydroxyl radicals. Here, one could integrate two functionalities to achieve appropriate band positions and desired bandgap of Zn-BTC. $Zn_3(BTC)_2(C_6H_5)$ has a PLD and LCD of 5.25 Å and 9.25 Å, respectively.

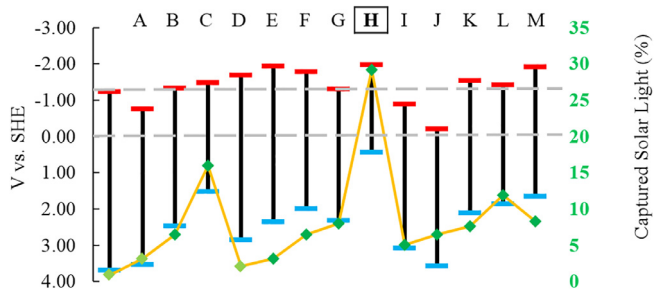

Fig. 6. Band energy plot of Zn-BTC and effect of functionalization using HSE06 functional versus the standard hydrogen electrode (SHE) potential.

In order to study the effectiveness of the selected material, $Zn_3(BTC)_2(C_6H_5)$ is compared to MIL-125(Ti) and its amine functionality. Recently, experimental work was carried out to study MIL-125(Ti) alongside some linker functionality towards nitrogen fixation (Huang et al., 2020). Although, the source of hydrogen in our case is molecular hydrogen, whereas water was used in the experiment by Huang et al., 2014. Nevertheless, here, we compare the parent structures and most successful functionalization, in terms of electronic properties, adsorption of N_2 and NH_3, heat of adsorption, diffusion and geometrical properties.

NH_2-MIL-125(Ti) was built by manually inserting the functionality, and only 1 linker is replaced with BDC-NH_2. It was shown the amine content of 1 per unit cell saturates the structure (Hendon et al., 2013). The process is followed by geometry optimization scheme in CP2K software using limited memory Broyden-Fletcher-Goldfarb (LBFGS) optimization algorithm (Byrd et al., 1995).

Table 2 lists all the properties that are used in the comparison between the four structures. From the conduction band perspective, the bandgap in Zn-BTC is highly negative, which facilitate the transition of the excited electrons to the nitrogen. In other words, electrons in the conduction band is accessible to nitrogen natural (thermodynamics). MC and MD simulations were performed using RASPA software (Dubbeldam et al., 2016), and details regarding the simulations are found in the supporting information document. Charge equilibration method implemented in RASPA package was used to assign points charges for Phenyl-Zn-BTC to study the contribution of the electrostatic interaction. It can be seen that the presence of functional groups affects the adsorption and heat of adsorption of studied gases. Zn-BTC catalyst has almost 1.8 higher Henry's constant than MIL-125(Ti). Nitrogen heat of adsorption at 1 bar is higher in the case of Zn-BTC and phenyl-Zn-BTC that Ti-based structures. It has to be noted that ammonia heat of adsorption is also increased, but it does not exceed physisorption limits. Adsorption isotherm at 298.15 K and heat of adsorption at different pressures [0.5-10 bar] are shown in Fig. 7. Similar plots are prepared for ammonia (Fig. S1).

The single gas diffusion coefficient is influenced by the presence of bulky functionalization as represent by a phenyl group. The nitrogen and ammonia diffusion coefficients in phenyl-Zn-BTC are 1.82E-05 cm^2/s and 1.13E-05 cm^2/s, respectively. It was revealed that diffusion computations employed in this work are costly because of the inclusion of adsorbate-host interactions. Fig. 8(a) and (b) show the RDF between N_2 and metal atom, respectively. A non-zero RDF histogram, at infinite dilution, is observed at 2.484 Å and 3.516 Å, in the case of phenyl-Zn-BTC and NH_2-MIL-125(Ti), respectively. The distance comparison highlights that nitrogen molecule is closer to the active site in the case of phenyl-Zn-BTC structure. Fig. S2 depicts the impact of pressure on the RDF between N_2 and Zn.

In addition, comparison between the structures from an environmental perspective is added, expanding the environmental impact beyond the metal site. In this analysis, the functional unit is 1 kg of the MOF. The boundary of the study involves the materials used in the production of the MOF. Use and recycling phases are not included as the comparison that is meant to compare the materials from an environmental point of view directly. GaBi software (Thinkstep, 2014) databases are used in the study to model the cradle-to-gate LCA. Nine impact categories are considered, which include GWP, acidification, toxicity, ozone and fossil depletion, and

Table 2
Calculated geometrical properties, adsorption and diffusion computations for comparison between MIL-125(Ti), NH2-MIL-125(Ti), Zn-BTC and Phenyl-Zn-BTC.

Structures		MIL-125 (Ti)	NH_2-MIL-125 (Ti)	Zn-BTC	Phenyl-Zn-BTC
Chemical composition		$C_{96}H_{56}O_{72}Ti_{16}$	$C_{96}H_{57}NO_{72}Ti_{16}$	$C_{72}H_{48}O_{48}Zn_{12}$	$C_{126}H_{108}O_{48}Zn_{12}$
Topology		Fcu		Tbo	
Density (kg/m^3)		786.74	832.09	887.23	1136.09
Void fraction		0.6791±0.0005	0.663±0.007	0.775±0.003	0.539±0.004
Accessible Surface Area (m^2/g)		2524±3	2230±2	2330+2	1113.8±0.7
HSE06	Bandgap	3.749	2.330	4.923	2.410
	Conduction Band	0.041	0.025	-1.249	-1.981
	Valance Band	3.789	2.354	3.675	0.429
PBE	Bandgap	2.772	1.430	3.488	1.528
	Conduction Band	0.369	0.334	-0.915	-1.642
	Valance Band	3.139	1.764	2.573	-0.114
N_2 Henry's constant (mol/kg/bar)		0.255±0.001	0.272±0.001	0.452±0.002	1.00±0.02
NH_3 Henry's constant (mol/kg/bar)		0.711±0.004	0.855±0.007	2.24±0.05	10.6±0.2
N_2 Diffusion Coefficient (cm^2/s)		1.944E-04±3E-07	1.112E-04±5E-07	1.08E-05±6E-07	1.82E-05±2E-07
NH_3 Diffusion Coefficient (cm^2/s)		1.81E-04±1E-06	1.25E-04±1E-06	2.0E-05±1E-06	1.13E-05±1E-07
Adsorption of N_2 at 1 bar (mol/kg)		0.251±0.001	0.229±0.005	0.350±0.003	0.561±0.006
Adsorption of NH_3 at 1 bar (mol/kg)		0.85±0.07	1.02±0.03	2.0±0.2	6.57±0.08
Heat of adsorption of N_2 at 1 bar (kJ/mol)		-10.68±0.2	-11.3±0.1	-13.8±0.13	-17.7±0.2
Heat of adsorption of NH_3 at 1 bar (kJ/mol)		-15.1±0.7	-16.5±0.2	-20±1	30.9±0.3
Heat of adsorption of N_2 at infinite dilution (kJ/mol)		-10.5±0.2	-11.1±0.2	-14.5±0.2	-20.5±0.3
Heat of adsorption of NH_3 at infinite dilution (kJ/mol)		13.1±0.5	14.1±0.4	21±1	27±2
Binding energy N_2 (kJ/mol)		-11.727±0.002	-13.639±0.001	-11.270±0.002	-12.073±0.001
Binding energy NH_3 (kJ/mol)		-13.236±0.0007	-14.026±0.002	-13.299±0.003	-25.124±0.001
Non-zero RDF N(atom)-N_2 and metal at infinite dilution (Å)		3.468	3.516	2.364	2.484
The first peak of RDF between N(atom)-N_2 and metal at infinite dilution (Å)		7.5	7.476	6.468	6.636

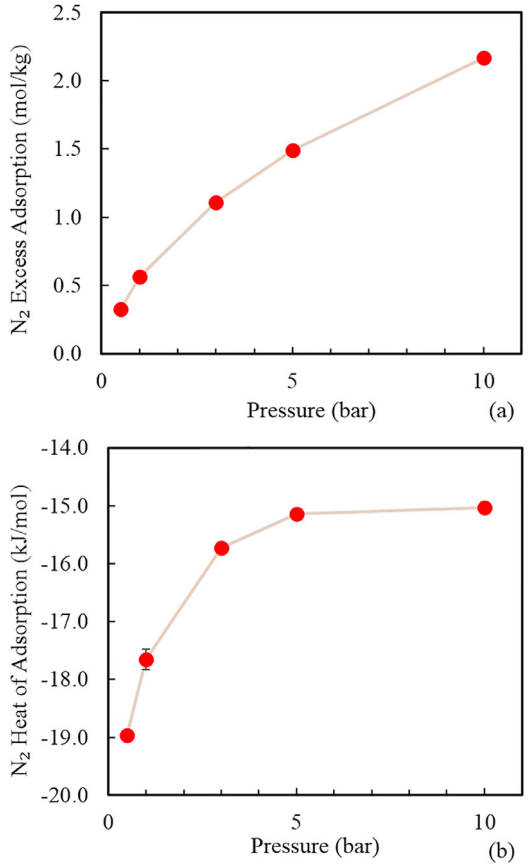

Fig. 7. (a) Excess adsorption isotherm of N_2 at 298.15 K (b) Isosteric heat of adsorption of N_2 at 298.15 K as a function of pressure. Error bars are smaller than the symbols' size.

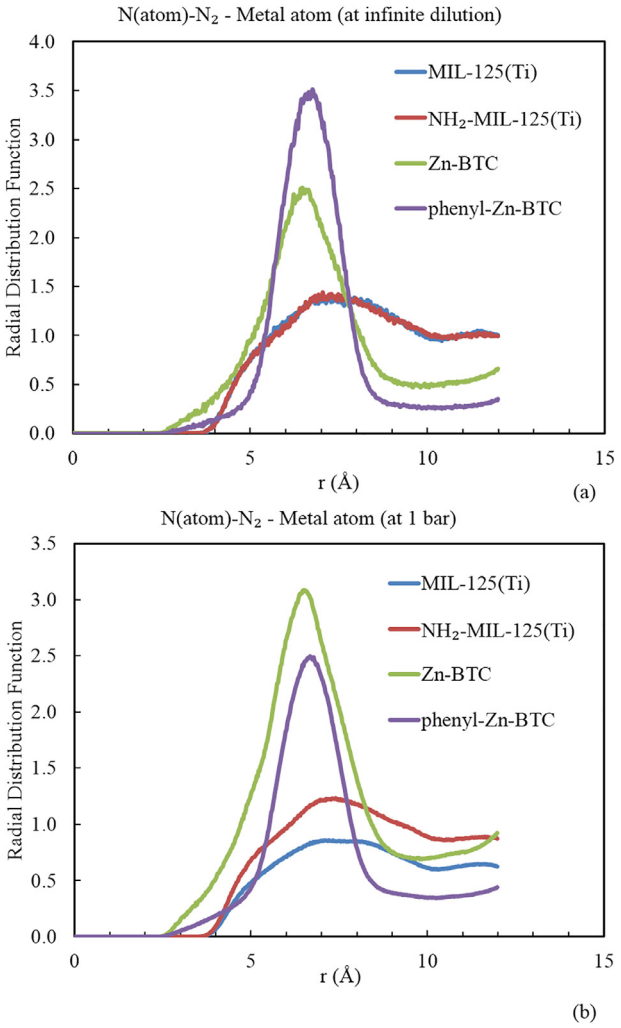

Fig. 8. . Radial distribution function between N atom in N_2 molecule and metal sites at (a) infinite dilution and (b) 1 bar and 298.15 K.

fine particulate matter formation. The amount of precursors to the production of the MOF is estimated from stoichiometry and assumed complete yield. MIL-125(Ti) is prepared from Titanium (IV)

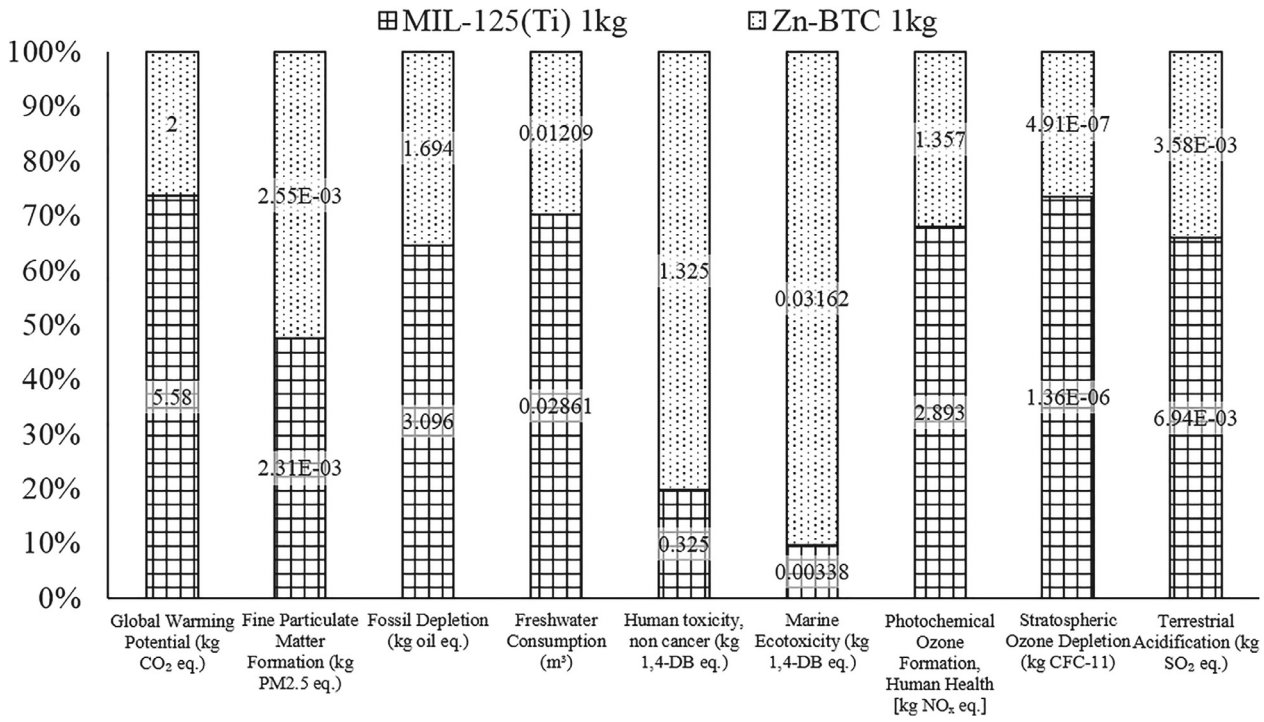

Fig. 9. Comparison between MIL-125 (Ti) and Zn-BTC in terms of several environmental impact categories.

butoxide ($Ti(C_4H_9O)_4$) and Terephthalic acid. On the other side, Zn-BTC is synthesized with zinc acetate and organic linker source in Trimesic acid. As a result of the unavailability of data concerning productions of $Ti(C_4H_9O)_4$, trimesic acid and zinc acetate, assumptions and approximations are used. One of the routes to the production of trimestic acid is through xylene mixture to produce mesitylene and later to trimestic acid. Zinc and acetic acid are used, per reaction stoichiometry, to estimate zinc acetate. Finally, Titanium isopropoxide is used to approximate $Ti(C_4H_9O)_4$ because of the similarity in the production scheme; both are produced via reaction of Titanium and appropriate alcohol; n-butanol and isopropanol, respectively.

Fig. 9 summarizes the environmental comparison in a 100% stacked bar chart. In all the studied categories, except for three (human toxicity, marine ecotoxicity and fine particulate matter formation), Zn-BTC is observed to have lower environmental burden relative to Ti-based MOF. Most of the increased impact is as a result of the Ti source. In the main category, GWP, the production of MIL-125(Ti) is associated with 5.58 kg CO_2 eq./kg of the material, which is almost three times the impact of Zn-BTC. As a result of xylene, Zn-BTC has a higher impact in toxicity categories: human toxicity and marine ecotoxicity. Both materials have approximately an equal impact when it comes to the fine particulate matter formation category. It is worth reiterating that the analysis is based on the production of material only; recycling and use phases are essential and may offset production values. In order to have a more holistic approach, one would appreciate the integration of environmental impact with bandgap value or adsorption computations.

Here, we highlight literature work on Zn-BTC based MOFs in catalytic applications that illustrate the stability of structures and shows different applications. Also, it demonstrates that such screening has the potential to open the doors for efficient use of materials in a different application than previously studied. MOF Zn-BTC is a structure in the HMOFs but has been synthesized and studied in the literature for various application. Three MOFs based on Zn-BTC (BIT101-103) was first synthesized and tested for the catalytic synthesis from propylene carbonate from

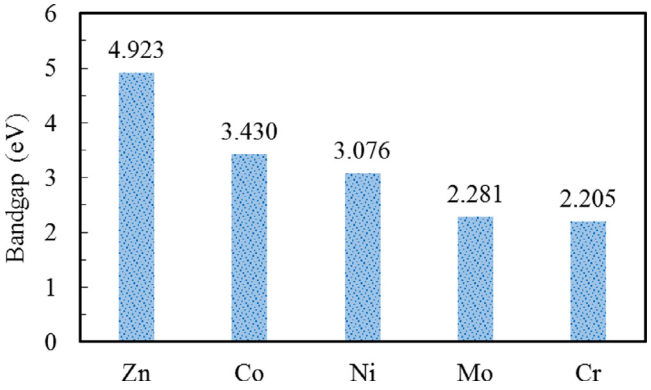

Fig. 10. The bandgap of M_3BTC_2 using HSE06 (M: Zn, Co, Ni, Co and Cr).

CO_2 and propylene epoxide (Huang et al., 2014). The open metal BTC based MOFs showed outstanding catalytic activity and regenerability. Also, Zn-BTC catalyst was used to catalyze the alkylation of toluene and tested for three cycles without activity loss (Farzaneh and Mortazavi, 2017). $Zn_3(BTC)_2$ was shown to be an environmentally benign, recyclable catalyst for the synthesis of regioselective ring-opening of epoxides sodium azide and thiocyanate anion (Sajjadifar et al., 2018).

Following the screening process, BTC based MOFs are highlighted as potential candidates because functionalization of the organic ligand resulted in appropriate bandgap positions. We transferred this potential and evaluated the bandgap of several M-BTC structures (Fig. 2). MOFs structures were optimized, starting from experimental structure (Rosen et al., 2019). Fig. 10 shows the bandgap of M-BTC using the same procedure aforementioned in this paper. Several metals are considered, which are Co, Ni, Mo, and Cr. The oxidation state of these metals in M-BTC is +2. It can be seen that the bandgap can be reduced to 2.205 as in the case of Cr-BTC, a 55% reduction relative to Zn-BTC. Group 6 metals (Cr and Mo) showed the lowest bandgaps among the studied structures.

In overall, design for efficient photocatalysts can be approached by combining metal substitution and ligand functionality effects.

4. Conclusion, outlook and challenges

The process of building a screening process of materials towards photocatalysis application has to be accompanied by experimental investigations to establish the connection between theory and experimentation. Several experimental parameters can be used to assess with heterogeneous photocatalytic systems are quantum yield, photocatalytic efficiency, turnover frequency and turnover number. These numbers are not possible to quantify using computations. Therefore, results from experiments have to be studied in synchronization with computation outcomes to verify and improve methodology preparation.

Experimental exploration of MOFs towards sustainable ammonia production is limited in the literature, which makes it challenging to include experimental knowledge to the screening. Transfer knowledge of similar induced chemical reactions such as water splitting and carbon dioxide reduction is crucial for rapid improvements in photocatalytic ammonia production systems. Improvement in the photocatalysts eventually feeds the electrochemical and photoelectrochemical cells applications. Moreover, photocatalytic systems contain solvents and other substances, besides promoters and co-catalysts. For a particular intriguing system, simulation of such highly complex systems might be needed to isolate each component's role in the process.

In this work, screening of HMOF library was accomplished considering several desired properties; including, structural, adsorption, environmental, cost, and optical properties. It was shown that the database used lacks the diversity of currently demonstrated in MOFs considering all layers of MOFs building blocks. Based on several steps, Zn-BTC with phenyl functionality satisfied all the preliminary screening criteria set namely, bandgap, bands positions, open metal site and environmental consideration. The selected structure was assessed through a combination of geometrical, adsorption, diffusion and electronic properties and compared with MIL-125(Ti) based MOF. Additionally, the environmental impact of these materials was evaluated using cradle-to-gate LCA that spans the production stage of materials. The results revealed that Zn-BTC catalysts are less harmful than Ti-based catalysts in six out of nine studied impact categories.

Supplementary document

Computational details on Monte Carlo and Molecular Dynamics simulations are available. The details include methods utilized and force field parameters. The document also includes adsorption isotherm of NH_3 at 298.15 K and radial distribution function of N(atom)-N_2 – Zn (phenyl-Zn-BTC) as a function of pressure which is obtained from adsorption simulations using GCMC simulations.

Declaration of Competing Interest

The authors declare that they have no known competing financial interests or personal relationships that could have appeared to influence the work reported in this paper. The authors declare that they have no conflict of interest.

Acknowledgement

This publication was made possible by an Award GSRA5-1-0513-18051 from Qatar National Research Fund (a member of Qatar Foundation). We are grateful to the High Performance Computing Center of Texas A&M University at Qatar for generous resource allocation. Open Access funding provided by the Qatar National Library. The contents herein are solely the responsibility of the authors.

Supplementary materials

Supplementary material associated with this article can be found, in the online version, at doi:10.1016/j.compchemeng.2020.107130.

References

Alvaro, M., Carbonell, E., Ferrer, B., Llabrés i Xamena, F.X., Garcia, H., Jun. 2007. Semiconductor Behavior of a Metal-Organic Framework (MOF). Chem. – A Eur. J. 13 (18), 5106–5112.
Armor, J.N., 2011. So you think you may have a better process: How can you define the value? Catal. Today 178 (1), 8–11.
Augugliaro, V., Palmisano, G., Palmisano, L., Soria, J., 2019. Heterogeneous Photocatalysis and Catalysis: An Overview of Their Distinctive Features. In: Marcì, G., Palmisano, L.B.T.-H.P. (Eds.), Heterogeneous Photocatalysis. Elsevier, pp. 1–24.
Azar, A.N.V., Velioglu, S., Keskin, S., May 2019. Large-Scale Computational Screening of Metal Organic Framework (MOF) Membranes and MOF-Based Polymer Membranes for H 2 /N 2 Separations. ACS Sustain. Chem. Eng. 7 (10), 9525–9536.
Banerjee, A., 2015. Photochemical nitrogen conversion to ammonia in ambient conditions with femos-chalcogels. J. Am. Chem. Soc. 137 (5), 2030–2034.
S.Bencic, "Ammonia Synthesis Promoted by Iron Catalysts Literature Report," Michigan State University, 2001.
Braslavsky Silvia, E, 2011. Glossary of terms used in photocatalysis and radiation catalysis (IUPAC Recommendations 2011). Pure and Applied Chemistry 83, 931.
Brown, K.A., 2016. Light-driven dinitrogen reduction catalyzed by a CdS:nitrogenase MoFe protein biohybrid. Science 352 (6284), 448–450 (80-.).
Butler, K.T., Hendon, C.H., Walsh, A., Feb. 2014. Electronic Chemical Potentials of Porous Metal–Organic Frameworks. J. Am. Chem. Soc. 136 (7), 2703–2706.
Byrd, R.H., Lu, P., Nocedal, J., Zhu, C., Sep. 1995. A Limited Memory Algorithm for Bound Constrained Optimization. SIAM J. Sci. Comput. 16 (5), 1190–1208.
Che, M., Mori, K., Yamashita, H., 2012. Elaboration, characterization and properties of silica-based single-site heterogeneous photocatalysts. Proc. Math. Phys. Eng. Sci. 468 (2143), 2113–2128.
Chen, X., Li, N., Kong, Z., Ong, W.-J., Zhao, X., 2018. Photocatalytic fixation of nitrogen to ammonia: state-of-the-art advancements and future prospects. Mater. Horizons 5 (1), 9–27.
Chung, Y.G., 2019. Advances, Updates, and Analytics for the Computation-Ready, Experimental Metal–Organic Framework Database: CoRE MOF. J. Chem. Eng. Data 64 (12), 5985–5998 Dec. 2019.
Chung, Y.G., Nov. 2014. Computation-Ready, Experimental Metal–Organic Frameworks: A Tool To Enable High-Throughput Screening of Nanoporous Crystals. Chem. Mater. 26 (21), 6185–6192.
Chung, Y.G., Oct. 2016. In silico discovery of metal-organic frameworks for precombustion CO 2 capture using a genetic algorithm. Sci. Adv. 2 (10), e1600909.
Cinar, Z., Mar. 2017. The Role of Molecular Modeling in TiO2 Photocatalysis. Molecules 22 (4), 556.
Dhakshinamoorthy, A., Asiri, A.M., García, H., Apr. 2016. Metal–Organic Framework (MOF) Compounds: Photocatalysts for Redox Reactions and Solar Fuel Production. Angew. Chemie Int. Ed. 55 (18), 5414–5445.
Dong, G., Ho, W., Wang, C., 2015. Selective photocatalytic N2 fixation dependent on g-C3N4 induced by nitrogen vacancies. J. Mater. Chem. A 3 (46), 23435–23441.
Dubbeldam, D., Calero, S., Ellis, D.E., Snurr, R.Q., 2016. RASPA: Molecular simulation software for adsorption and diffusion in flexible nanoporous materials. Mol. Simul. 42 (2), 81–101.
Emery, A.A., Wolverton, C., Dec. 2017. High-throughput DFT calculations of formation energy, stability and oxygen vacancy formation energy of ABO3 perovskites. Sci. Data 4 (1), 170153.
European Commission (EC), "Report on Critical Raw Materials for the EU; Report of the Ad-hoc Working Group on defining critical raw materials," Brussels, Belgium, 2014.
Farzaneh, F., Mortazavi, S.S., 2017. Zn metal organic framework as a heterogeneous catalyst for the alkylation of toluene with benzyl bromide. React. Kinet. Mech. Catal. 120 (1), 333–344.
Frenkel, D., Smit, B., 2002. Understanding molecular simulation: from algorithms to applications.
Gilbert, P., Thornley, P., 2010. Energy and carbon balance of ammonia production from biomass gasification. Bio-Ten Conference.
Goedecker, S., Teter, M., Hutter, J., Jul. 1996. Separable dual-space Gaussian pseudopotentials. Phys. Rev. B 54 (3), 1703–1710.
Gomes Silva, C., Luz, I., Llabrés i Xamena, F.X., Corma, A., García, H., Sep. 2010. Water Stable Zr–Benzenedicarboxylate Metal–Organic Frameworks as Photocatalysts for Hydrogen Generation. Chem. – A Eur. J. 16 (36), 11133–11138.
Gomez, D.A., Toda, J., Sastre, G., 2014. Screening of hypothetical metal–organic frameworks for H 2 storage. Phys. Chem. Chem. Phys. 16 (35), 19001–19010.
Graedel, T.E., Jan. 2012. Methodology of Metal Criticality Determination. Environ. Sci. Technol. 46 (2), 1063–1070.

Grande, C.A., Blom, R., Spjelkavik, A., Moreau, V., Payet, J., Dec. 2017. Life-cycle assessment as a tool for eco-design of metal-organic frameworks (MOFs). Sustain. Mater. Technol. 14, 11–18.
Guidon, M., Hutter, J., VandeVondele, J., Aug. 2010. Auxiliary Density Matrix Methods for Hartree−Fock Exchange Calculations. J. Chem. Theory Comput. 6 (8), 2348–2364.
Harper, E.M., Aug. 2015. Criticality of the Geological Zinc, Tin, and Lead Family. J. Ind. Ecol. 19 (4), 628–644.
Hartwigsen, C., Goedecker, S., Hutter, J., Aug. 1998. Relativistic separable dual-space Gaussian pseudopotentials from H to Rn. Phys. Rev. B 58 (7), 3641–3662.
Hasnip, P.J., Refson, K., Probert, M.I.J., Yates, J.R., Clark, S.J., Pickard, C.J., Mar. 2014. Density functional theory in the solid state. Philos. Trans. R. Soc. A Math. Phys. Eng. Sci. 372 (2011), 20130270.
Hendon, C.H., Jul. 2013. Engineering the Optical Response of the Titanium-MIL-125 Metal–Organic Framework through Ligand Functionalization. J. Am. Chem. Soc. 135 (30), 10942–10945.
Hohenberg, P., Kohn, W., Nov. 1964. Inhomogeneous Electron Gas. Phys. Rev. 136, B864–B871 3B.
Horiuchi, Y., Oct. 2012. Visible-Light-Promoted Photocatalytic Hydrogen Production by Using an Amino-Functionalized Ti(IV) Metal–Organic Framework. J. Phys. Chem. C 116 (39), 20848–20853.
Hu, S., Zhang, W., Bai, J., Lu, G., Zhang, L., Wu, G., 2016. Construction of a 2D/2D g-C3N4/rGO hybrid heterojunction catalyst with outstanding charge separation ability and nitrogen photofixation performance via a surface protonation process. RSC Adv 6 (31), 25695–25702.
Huang, X., 2014. Zn-BTC MOFs with active metal sites synthesized via a structure-directing approach for highly efficient carbon conversion. Chem. Commun. 50 (20), 2624–2627.
Huang, H., Jun. 2020. Toward visible-light-assisted photocatalytic nitrogen fixation: A titanium metal organic framework with functionalized ligands. Appl. Catal. B Environ. 267, 118686.
Hutter, J., Iannuzzi, M., Schiffmann, F., VandeVondele, J., Jan. 2014. CP2K: atomistic simulations of condensed matter systems. Wiley Interdiscip. Rev. Comput. Mol. Sci. 4 (1), 15–25.
Jiang, J., Apr. 2019. Computational screening of metal−organic frameworks for CO2 separation. Curr. Opin. Green Sustain. Chem. 16, 57–64.
Krukau, A.V., Vydrov, O.A., Izmaylov, A.F., Scuseria, G.E., Dec. 2006. Influence of the exchange screening parameter on the performance of screened hybrid functionals. J. Chem. Phys. 125 (22), 224106.
Lashgari, M., Zeinalkhani, P., 2018. Ammonia photosynthesis under ambient conditions using an efficient nanostructured FeS 2 /CNT solar-energy-material with water feedstock and nitrogen gas. Nano Energy 48, 361–368.
Leach, A.R., 2001. Molecular Modelling: Principles and Applications. Pearson/Prentice Hall, Harlow, England.
Leonat, L., Sbârcea, G., Branîoi, I.V., 2013. Cyclic voltammetry for energy levels estimation of organic materials. UPB Sci. Bull. Ser. B Chem. Mater. Sci. 75 (3), 111–118.
Li, Guoqiang, Li, Feifei, Liu, Jianxin, Fan, Caimei, 2020. Fe-based MOFs for photocatalytic N2 reduction: Key role of transition metal iron in nitrogen activation. Journal of Solid State Chemistry 285. doi:10.1016/j.jssc.2020.121245.
Liu, X., Cheng, J., Sprik, M., Jan. 2015. Aqueous Transition-Metal Cations as Impurities in a Wide Gap Oxide: The Cu 2+ /Cu + and Ag 2+ /Ag + Redox Couples Revisited. J. Phys. Chem. B 119 (3), 1152–1163.
Martin, M.G., Siepmann, J.I., 1998. Transferable Potentials for Phase Equilibria. 1. United-Atom Description of n -Alkanes. J. Phys. Chem. B 102 (97), 2569–2577.
Mori-Sánchez, P., Cohen, A.J., Yang, W., Nov. 2006. Many-electron self-interaction error in approximate density functionals. J. Chem. Phys. 125 (20), 201102.
Mouchaham, G., Wang, S., Serre, C., 2018. The Stability of Metal-Organic Frameworks. In: *Metal-Organic Frameworks*, Weinheim. Wiley-VCH Verlag GmbH & Co. KGaA, Germany, pp. 1–28.
N. R. C., 2008. Committee on Critical Mineral Impacts of the U.S. Economy, Committee on Earth Resources, "Minerals, Critical Minerals, and the U.S. Economy. The National Academies Press, Washington, DC.
Nasalevich, M.A., Apr. 2016. Electronic origins of photocatalytic activity in d0 metal organic frameworks. Sci. Rep. 6 (1), 23676.
Nassar, N.T., Jan. 2012. Criticality of the Geological Copper Family. Environ. Sci. Technol. 46 (2), 1071–1078.
Navalón, S., García, H., 2018. MOFs as Photocatalysts. Metal-Organic Frameworks: Application in Separations and Catalysis, 1st ed. Germany: Wiley-VCH Verlag GmbH & Co. KGaA, Weinheim.
Nuss, P., Eckelman, M.J., Jul. 2014. Life Cycle Assessment of Metals: A Scientific Synthesis. PLoS One 9 (7), e101298.
Nuss, P., Harper, E.M., Nassar, N.T., Reck, B.K., Graedel, T.E., Apr. 2014. Criticality of Iron and Its Principal Alloying Elements. Environ. Sci. Technol. 48 (7), 4171–4177.
Ongari, D., Yakutovich, A.V., Talirz, L., Smit, B., Oct. 2019. Building a Consistent and Reproducible Database for Adsorption Evaluation in Covalent–Organic Frameworks. ACS Cent. Sci. 5 (10), 1663–1675.
Oshikiri, T., Ueno, K., Misawa, H., 2016. Selective Dinitrogen Conversion to Ammonia Using Water and Visible Light through Plasmon-induced Charge Separation. Angew. Chemie - Int. Ed. 55 (12), 3942.
Perdew, J.P., Ernzerhof, M., Burke, K., Dec. 1996. Rationale for mixing exact exchange with density functional approximations. J. Chem. Phys. 105 (22), 9982–9985.
Perdew, J.P., Burke, K., Ernzerhof, M., Feb. 1997. Generalized Gradient Approximation Made Simple. Phys. Rev. Lett. 78 (7), 1396.
Petrovic, I., Navrotsky, A., Davis, M.E., Zones, S.I., Dec. 1993. Thermochemical study of the stability of frameworks in high silica zeolites. Chem. Mater. 5 (12), 1805–1813.
Pham, H.Q., Mai, T., Pham-Tran, N.-N., Kawazoe, Y., Mizuseki, H., Nguyen-Manh, D., Mar. 2014. Engineering of Band Gap in Metal–Organic Frameworks by Functionalizing Organic Linker: A Systematic Density Functional Theory Investigation. J. Phys. Chem. C 118 (9), 4567–4577.
Qiao, Z., Peng, C., Zhou, J., Jiang, J., 2016. High-throughput computational screening of 137953 metal–organic frameworks for membrane separation of a CO 2 /N 2 /CH 4 mixture. J. Mater. Chem. A 4 (41), 15904–15912.
Rosen, A.S., Notestein, J.M., Snurr, R.Q., Apr. 2019. Structure–Activity Relationships That Identify Metal–Organic Framework Catalysts for Methane Activation. ACS Catal 9 (4), 3576–3587.
Sajjadifar, S., Arzehgar, Z., Khoshpoori, S., May 2018. Zn3(BTC)2 as a Metal–Organic Framework and Effective Catalyst for the Regioselective β-Azidoalcohols and β-Thiocyanohydrins of Epoxides in Water. J. Inorg. Organomet.Polym.Mater. 28 (3), 837–846.
Silva, C.G., Corma, A., García, H., 2010. Metal–organic frameworks as semiconductors. J. Mater. Chem. 20 (16), 3141–3156.
"The CP2K developers group," 2008. [Online]. Available: http://www.cp2k.org.
Thinkstep, AG, 2014. GaBi 6 software and databases. Leinfelden-Echterdingen, Germany.
Thomas, J.M., Thomas, W.J., 2015. In: Weinheim, Re. (Ed.), Second. Wiley-VCH Verlag GmbH & Co. KGaA, Germany.
Turner, C.H., Johnson, J.K., Gubbins, K.E., Jan. 2001. Effect of confinement on chemical reaction equilibria: The reactions 2NO⇔(NO)2 and N2+3H2⇔2NH3 in carbon micropores. J. Chem. Phys. 114 (4), 1851–1859.
Turro, N.J., Ramamurthy, V., Scaiano, J.C., 2010. Principles of Molecular Photochemistry: An Introduction. University Science Books, New York.
VandeVondele, J., Hutter, J., Sep. 2007. Gaussian basis sets for accurate calculations on molecular systems in gas and condensed phases. J. Chem. Phys. 127 (11), 114105.
Wang, J.-L., Wang, C., Lin, W., Dec. 2012. Metal–Organic Frameworks for Light Harvesting and Photocatalysis. ACS Catal 2 (12), 2630–2640.
Wei, X., Wang, K.-X., Guo, X.-X., Chen, J.-S., Jul. 2012. Single-site photocatalysts with a porous structure. Proc. R. Soc.A Math. Phys. Eng. Sci. 468 (2143), 2099–2112.
Willems, T.F., Rycroft, C.H., Kazi, M., Meza, J.C., Haranczyk, M., Feb. 2012. Algorithms and tools for high-throughput geometry-based analysis of crystalline porous materials. Microporous Mesoporous Mater 149 (1), 134–141.
Wilmer, C.E., Farha, O.K., Bae, Y.S., Hupp, J.T., Snurr, R.Q., 2012. Structure-property relationships of porous materials for carbon dioxide separation and capture. Energy Environ. Sci. 5 (12), 9849–9856.
Wilmer, C.E., Feb. 2012. Large-scale screening of hypothetical metal–organic frameworks. Nat. Chem. 4 (2), 83–89.
Ye, J., Johnson, J.K., May 2015. Design of Lewis Pair-Functionalized Metal Organic Frameworks for CO 2 Hydrogenation. ACS Catal 5 (5), 2921–2928.
Zhang, L., Siepmann, J.I., 2010. Development of the trappe force field for ammonia. Collect. Czechoslov. Chem. Commun. 75 (5), 577–591.
Zhang, H., Nai, J., Yu, L., (David) Lou, X.W., Sep. 2017. Metal-Organic-Framework-Based Materials as Platforms for Renewable Energy and Environmental Applications. Joule 1 (1), 77–107.